Elastic and hierarchical porous carbon nanofibrous membranes incorporated with $NiFe_2O_4$ nanocrystals for high efficient capacitive energy storage

Jianlong Ge [a], Gang Fan [a], Yang Si [a], Jianxin He [b], Hak-Yong Kim [c], Bin Ding [a,b,*], Salem S. Al-Deyab [d,*], Mohamed El-Newehy [d,e], Jianyong Yu [a,*]

[a] Key Laboratory of Textile Science & Technology, Ministry of Education, College of Textiles, Donghua University, Shanghai 201620, China.

[b] College of Textiles, Zhongyuan University of Technology, Zhengzhou, 450007, China.

[c] Department of BIN Fusion Technology, Chonbuk National University, Jeonju 561-756, Republic of Korea.

[d] Petrochemical Research Chair, Department of Chemistry, College of Science, King Saud University, Riyadh 11451, Saudi Arabia.

[e] Department of Chemistry, Faculty of Science, Tanta University, Tanta 31527, Egypt.

Email: binding@dhu.edu.cn, ssdeyab@ksu.edu.sa, and yujy@dhu.edu.cn.

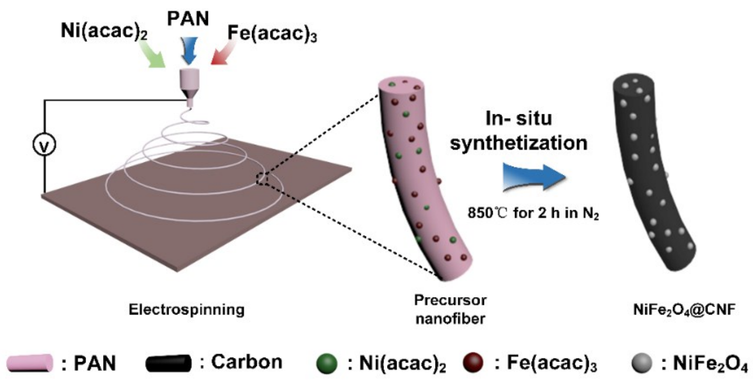

Fig. S1 Schematic diagram illustrating the fabrication of $NiFe_2O_4$ doped CNFs.

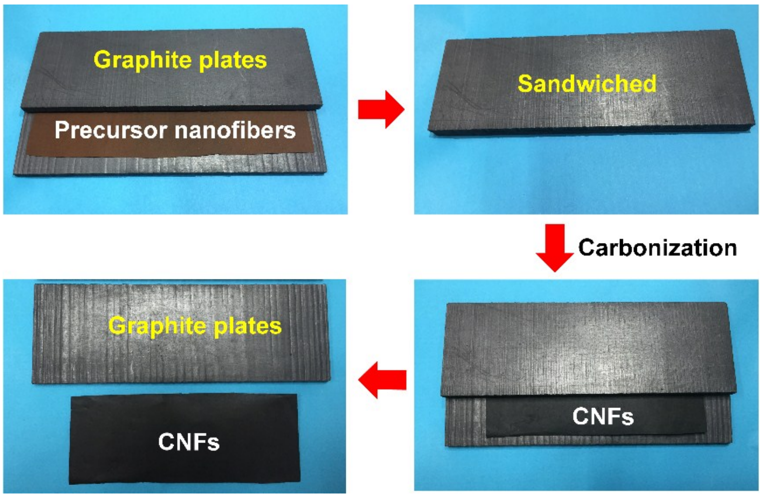

Fig. S2 Photos showing the carbonization process of CNFs.

Table S1. Composition and property of different electrospinning solutions.

Samples	PAN (wt%)	Salts (wt%)	Viscosity (cps)	Conductivity ($\mu S\ m^{-1}$)
0 wt% salts/PAN	8	0	403	62
1 wt% salts/PAN	8	1	430	81
5 wt% salts/PAN	8	5	446	99
10 wt% salts/PAN	8	10	438	119

Table S2 The summary of pore structure parameters of relevant CNF membranes.

Samples	S_{BET}[a] ($m^2\ g^{-1}$)	S_{meso}[b] ($m^2\ g^{-1}$)	V_{total}[c] ($cm^3\ g^{-1}$)	V_{meso}[d] ($cm^3\ g^{-1}$)	PVF_{meso}[e] (%)	D_{av}[f] (nm)
0 wt% salts/PAN-CNF	353	9	0.19	0.01	5.3	2.1
1 wt% salts/PAN-CNF	466	50	0.27	0.05	18.5	2.3
5 wt% salts/PAN-CNF	493	112	0.31	0.15	48.5	2.5
10 wt% salts/PAN-CNF	442	169	0.37	0.20	54.1	3.3

[a] Total surface area was calculated by the BET method.

[b] Mesopore surface area was calculated by the Barret, Joyner, and Halenda (BJH) method.

[c] Total pore volume was estimated was calculated at P/P_0= 0.99.

[d] V_{meso} was calculated by the BJH method.

[e] PVF_{meso} indicates the pore volume fraction of mesopores.

[f] Average pore width was estimated by the BET method (4V/A by BET).

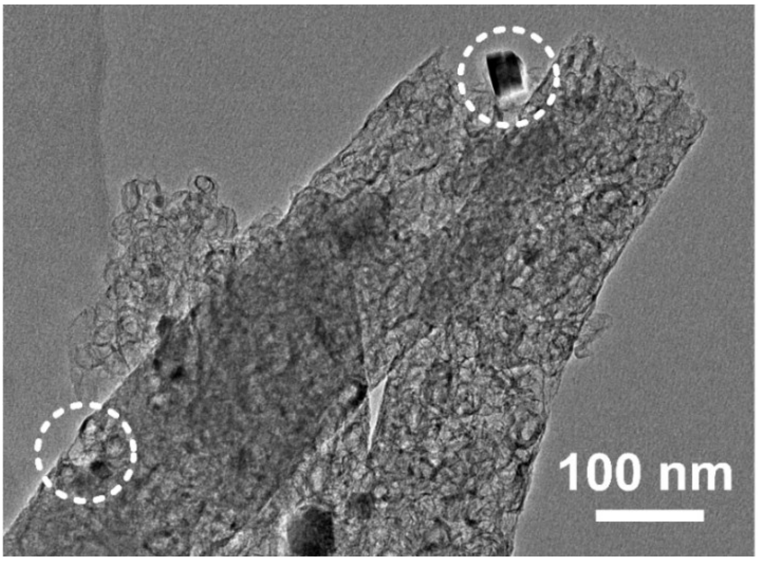

Fig. S3 FE-TEM image of relevant CNF derived from precursor nanofibers with salts content of 10 wt%.

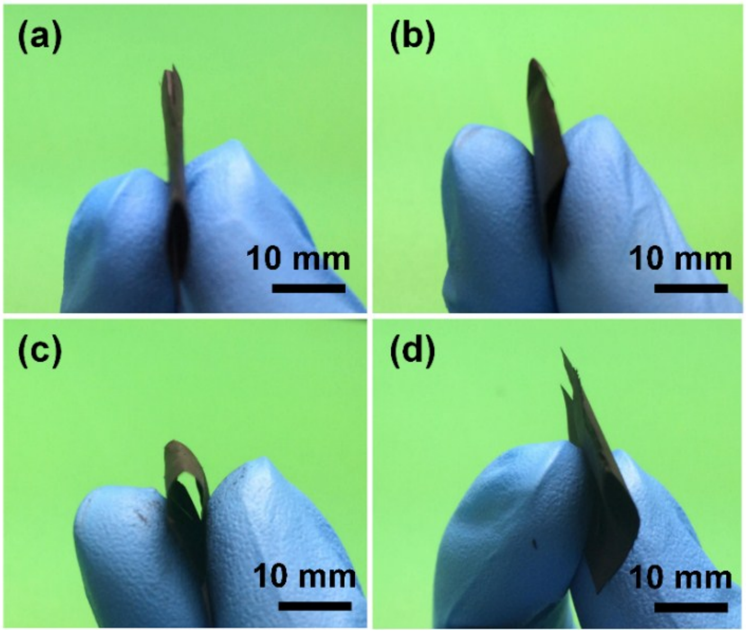

Fig. S4 Different elasticity of CNF membranes derived from precursor nanofibers with various concentrations of salts: (a) 0, (b) 1, (c) 5, and (d) 10 wt%.

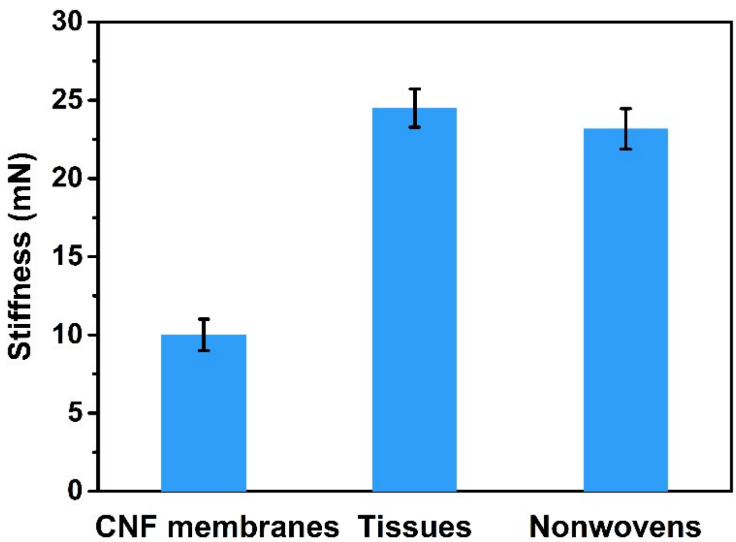

Fig. S5 Stiffness values of elastic CNF membranes, commercial polymer based tissue paper and nonwovens.

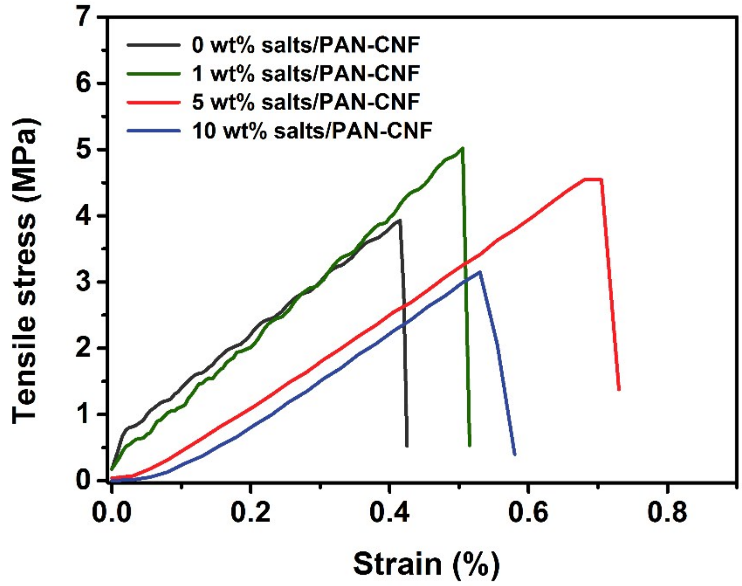

Fig. S6 Stress-strain curves of CNF membranes derived from precursor fibers with various concentration of salts.

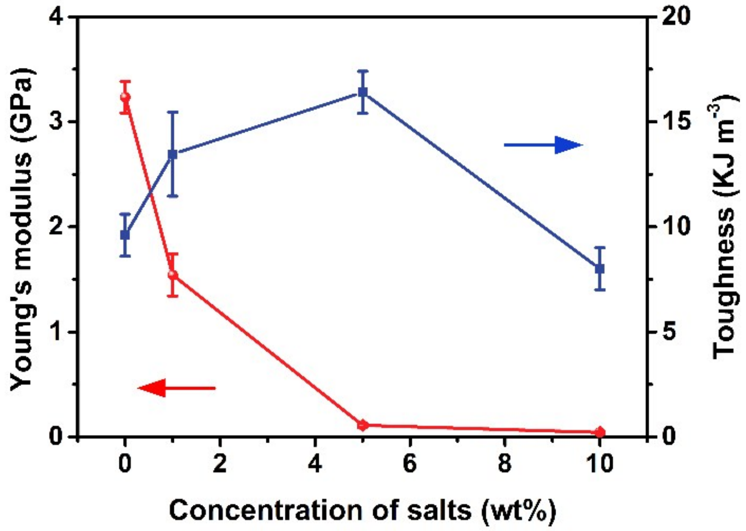

Fig. S7 Corresponding Young's modulus and toughness of CNF membranes derived from precursor fibers with different salts contents

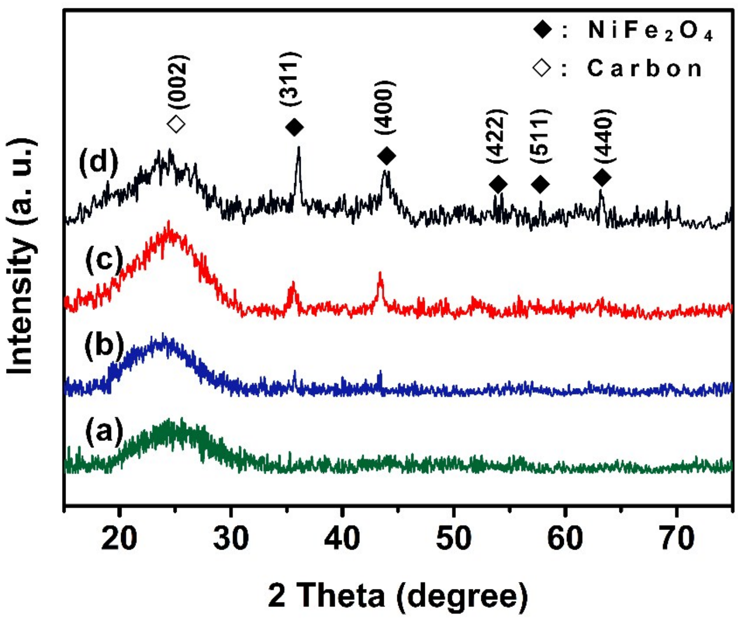

Fig. S8 Representative XRD patterns of CNF derived from precursor fibers with salts contents of (a) 0, (b) 1, (c) 5, and (d) 10 wt%.

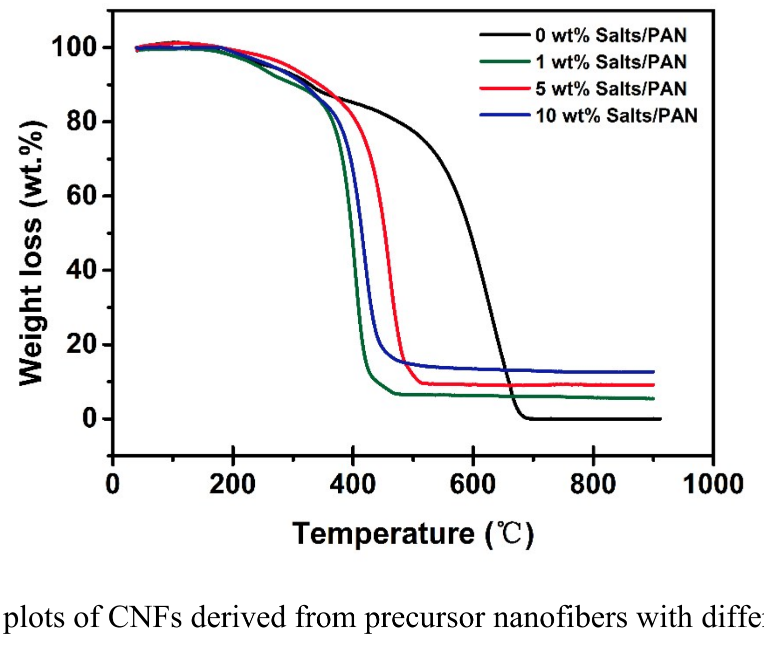

Fig. S9 TGA plots of CNFs derived from precursor nanofibers with different salts content in air condition.

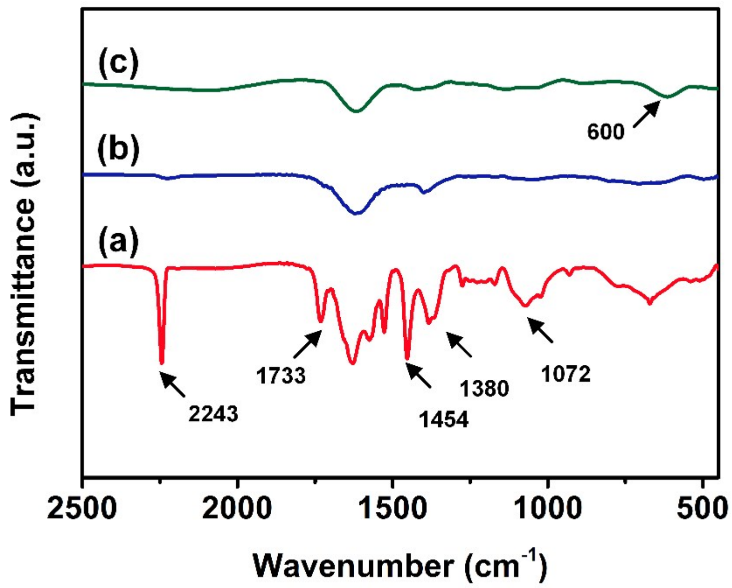

Fig. S10 FT-IR plots of (a) pristine precursor nanofibers; (b) Stabilized precursor nanofibers; (c) $NiFe_2O_4$ doped CNF.

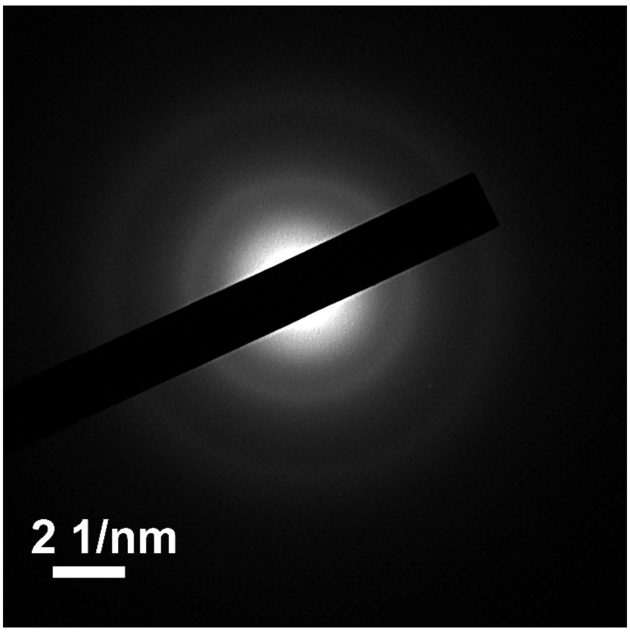

Fig. S11 SAED pattern of CNF derived from precursor nanofibers with 5 wt% salts content.

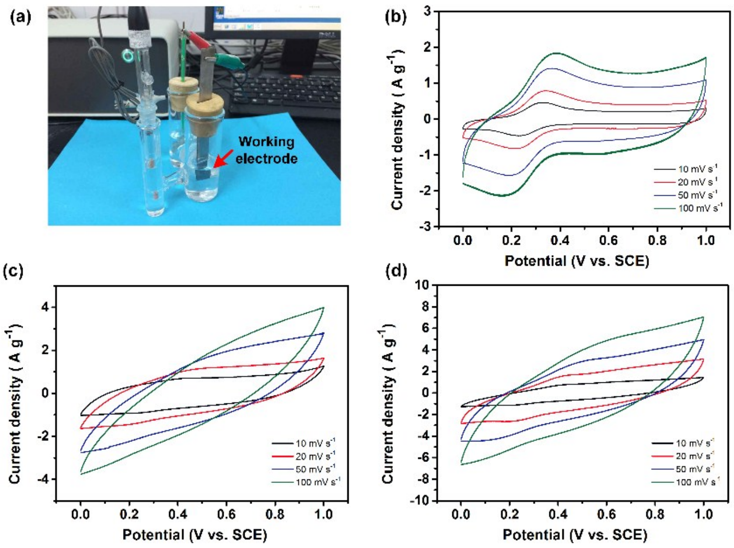

Fig. S12 (a) Digital photo of the three electrode setup used for the testing of electrical performance**,** and (b) CV curves of $NiFe_2O_4$, (c) CNF, and (d) $NiFe_2O_4$ doped CNF at different scan rates in a typical three electrodes setup.

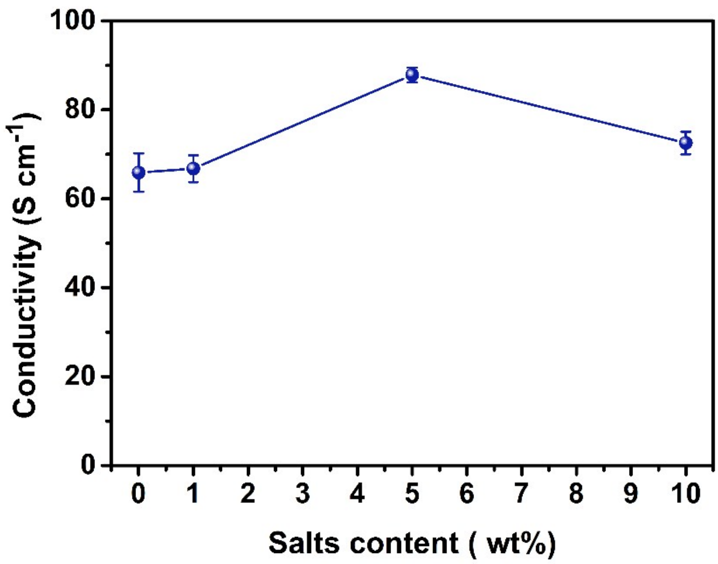

Fig. S13 Conductivity of CNF membranes derived from precursor nanofibers with different content of salts.

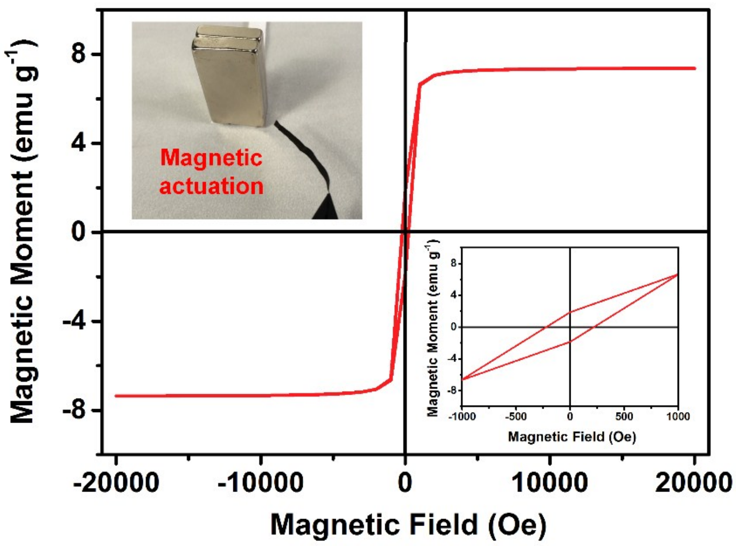

Fig. S14 Magnetic property of CNF membranes derived from precursor fibers with salts content of 5 wt% measured at 300 K.